Determination of the diamond wheel structure in high-speed grinding using nanoindentation techniques: experimental and numerical simulation

A.G. Mamalis,[1,*] A.I. Grabchenko,[2] D.V. Romashov,[2] D.O. Fedorenko,[2] D. Lagoudas,[3] V.A. Fedorovich[2] and J. Kundrak[4]

[1] *Project Centre for Nanotechnology and Advanced Engineering (PC-NAE), NCSR "Demokritos", Athens, Greece*
[2] *Department of Integrated Engineering Techniques named after M.F. Semko, National Technical University "Kharkov Polytechnic Institute", Kharkov, Ukraine*
[3] *Aerospace Engineering Department, Texas A&M University, College Station, Texas, USA*
[4] *Department of Production Engineering, University of Miskolc, Hungary*

Grinding at high speeds (over 80 m/s) is a complex process requiring deep understanding for successful deployment. This article describes ways of improving the integrity of the structure of diamond grinding wheels for high-speed regimes using nanoindentation techniques, as well as the prospects for their solution, using mathematical modelling methods.

Keywords: binder, destructive stress, diamond grains, finite element method, high speed grinding, nanoindentation

1. Introduction

The design of the grinding wheel is as critical to the success of the abrasive product as the other components of the composite. "Design" includes the physical dimensions, the form produced on the abrasive surface, the hub (material especially with respect to its ability to withstand rotational and thermal stresses), the rotational error, dynamic balance and chemical resistance.

Grinding wheels can range in size from a thickness of several micrometres (for silicon wafer dicing) to a metre wide (for wood pulp grinding). Although the shape of the active abrasive surface is usually trued into the wheel, there has been extensive research carried out

* Corresponding author. E-mail: mamalis@ims.demokritos.gr

to produce near-net shaped, vitrified core wheels for superabrasive products, diminishing wasted abrasive.

Rotational stresses during high-speed grinding can lead to failure if the hub is not correctly designed. The use of finite element method—FEM analysis—design of the hub and the number of segments (in the case of superabrasive wheels),[1] together with the improved guarding of modern machines, has reduced the risk of injury due to incorrect wheel design. Alternatively, composite wheel hubs (i.e., carbon fibre based) have been researched and are now commercially available. The rotational precision of single-layer superabrasive is generally a function of the grain size distribution and the electroplating method. However, microtruing of these wheels by 2–4 μm is possible in order to reduce the surface roughness produced.

High-speed processing modes require appropriate equipment with the corresponding spindles, grinding tools, subsystems and rigidity. One of the most important tasks for the wider use of high-speed diamond grinding is to adequately deal with security issues, including the integrity of wheels under the action of large centrifugal forces, and their stability at high speeds.[1–4] The creation of 3D modelling methodology for predicting the behaviour of the tool in all major phases of its life cycle is one of the least expensive ways to increase its efficiency and, hence, the efficiency of the treatment process. This study examined the 3D modelling of industrial strength tests of diamond wheels undergoing stresses arising in the process of high-speed grinding.[5–8] Model experiments in this case make it possible to establish the dependence between the integrity of wheels and a wide range of materials and forms of the tool. Such results are extremely difficult to obtain via the requisite large number of field experiments, due to the high cost of the testing equipment.[2,3,9] The article also describes the simulation of nanoindentation of different types of binders of diamond wheels.

2. Structure of a diamond grinding wheel

Grinding wheels and abrasive segments fall under the general category of "bonded abrasive tools". Such tools consist of hard abrasive grains or grits, which do the cutting, held in a softer

---

[1] E. Brinksmeier, J.C. Aurich and E. Govekar. Advances in modeling and simulation of grinding processes. *Annals of the CIRP* **57** (2006) 667–696.

[2] J. Webster and M. Tricard. Innovations in abrasive products for precision grinding. *Annals of the* CIRP **53/2** (2004) 597–617.

[3] F. Klocke. Characterization of vitrified cBN grinding wheels. *4th Int. Machining and Grinding Conf.*, SME, Michigan (2001).

[4] J.F.G. Oliveira, E.J. Silva and C. Guo. Industrial challenges in grinding. *Annals of the* CIRP **58** (2009) 663–680.

[5] E. Uhlmann and L. Hochschild. Tool optimization for high speed grinding. *Production Engineering* **7** (2013) 185–193.

[6] T.W. Hwang, C.J. Evans and S. Malkin. An investigation of high speed grinding with electroplated diamond wheels. *Annals of the* CIRP **49/1** (2000) 245–248.

[7] Z. Shi and S. Malkin. Investigation of grinding with electroplated cBN wheels. *Annals of the* CIRP **53/1** (2003) 267–270.

[8] N. Funayama and J. Matsuda. Development of high-performance cBN and diamond grinding wheels for high-speed grinding. *New Diamond and Frontier Carbon Technology* **15** (2005) 173–180.

[9] N. Barlow and M. Jackson. Mechanical design of high-speed vitrified cBN grinding wheels. *Proc. IMEC*, pp. 568–570. Univ. of Connecticut (1996).

bonding matrix. Depending on the particular type of bond, the space between the abrasive particles may only be partially filled, leaving gaps and porosity, or completely filled with binder. Aside from abrasive and bond material, fillers and grinding aid materials may also be added. The properties and performance of bonded abrasive tools depend on the type of abrasive grain material, the size of the grit, the bond material, the properties of the abrasive and bond, and the porosity (Figure 1).

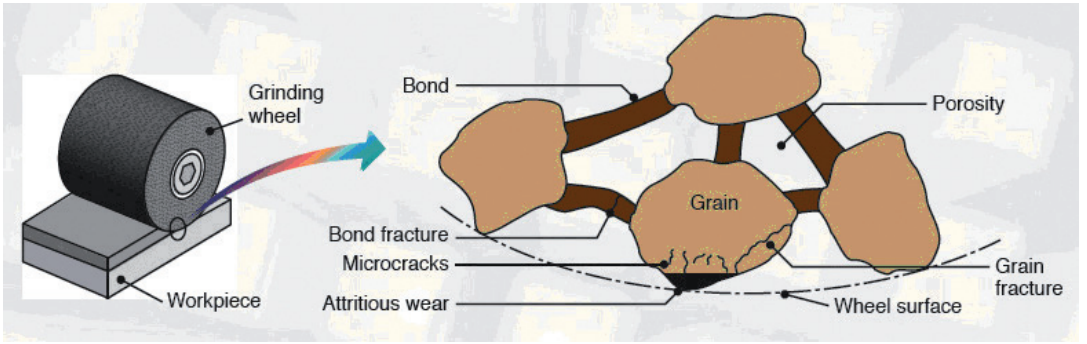

Figure 1. Schematic illustration of a physical model of a grinding wheel, showing its structure and grain wear and fracture patterns

The salient structural feature is basically the spacing between the abrasive grains. An "open" structure might be, for example, 38% by volume of diamond grains while 60% of diamond grains in the wheel would be a "closed" structure. Here again, the structure depends on a variety of factors, not the least of which is how difficult the workpiece material is to grind. One would think that a closer spacing would make a tougher wheel but this is only true up to a point: the fewer the bonds holding the individual abrasive grains, the softer the wheel. Also, the same holds true for a very open structure: if the grains are widely spaced there are fewer grains to grind with but a greater number of bonds holding each grain. Grinding wheel engineers will typically adjust the bond strength depending on the application.

3. Numerical simulation of the nanoindentation test

The finite element method (FEM) is a continuum simulation technique in structural mechanics. The associated models have the ability to simulate the loading–unloading curves and the development of plastic deformation during indentation and to extract material properties like hardness and elastic modulus from the tests. Here the indentation processes were simulated with the ABAQUS finite element software program taking input data from compression testing of Bakelite and iron-based binders of diamond wheels. The iron-based binder one of the most common binders in production in the Ukraine. The composition includes: lead 3–10%, nickel 2–5%, boron 0.5–3%, titanium 2–12%, aluminium 2–4%. The rest is iron and an insignificant amount of impurities. The hardness and elastic modulus were measured using this model (Figure 2).

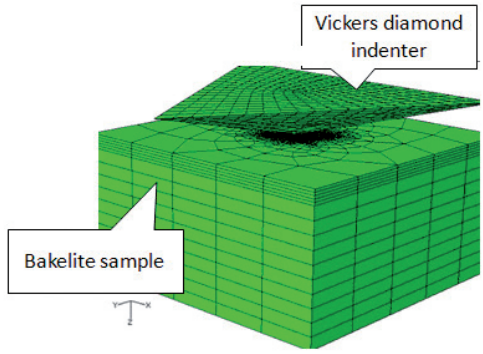

Figure 2. Simulation of nanoindentation using a finite element model.

4. Experimental validation of the nanoindentation model

The goal of the majority of nanoindentation tests is to extract the elastic modulus and hardness of the specimen material from load–displacement measurements.[10,11] Conventional indentation hardness tests involve the measurement of the size of a residual plastic impression in the specimen as a function of the indenter load. This provides a measure of the area of contact for a given load. In a nanoindentation test, the size of the residual impression is often only a few micrometres and this makes it very difficult to obtain a direct measure using optical techniques. The depth of penetration beneath the specimen surface is measured as the load is applied to the indenter. The known geometry of the indenter then allows the size of the area of contact to be determined.[10] The procedure also allows for the modulus of the specimen material to be obtained from a measurement of the "stiffness" of the contact; that is, the rate of change of load and depth. The reload indentation elastic modulus for fused binders was equivalent to the tensile test elastic modulus from reference literature.

The Fischerscope HM2000 (Figure 3) is designed to measure microhardness as well as further intrinsic material data, such as the Martens or Vickers hardness and the modulus of elasticity. The universal hardness is determined according to DIN EN ISO 14577. A Vickers or Berkovich pyramid is used as an indenter and is pressed into the material or coating whose hardness is to be determined. The load applied onto the sample increases continually until its maximum value is reached. The test load then diminishes. However, a mark of the indenter is left in the sample. Throughout the entire load cycle, the indentation depth is measured.

The hardness is derived from the maximum load F applied and the mark's area $A = f(h)$, where h is nanoindentation depth, as follows:

$$\mathrm{HM} = F/A \tag{1}$$

where HM is indentation hardness. The geometry of the indenter and the shape of the mark left by the indenter in the material after the indentation process are, of course, taken into consideration in the calculations of the mark's area.

[10] E.S. Berkovich. Three-faceted diamond pyramid for micro-hardness testing. *Industrial Diamond Rev.* **11** (1951) 129–133.
[11] D.B. Marshall, T. Noma and A.G. Evans. A simple method for determining elastic modulus-to-hardness ratios using Knoop indentation measurements. *J. Am. Ceram. Soc.* **65** (1980) C175–C176.

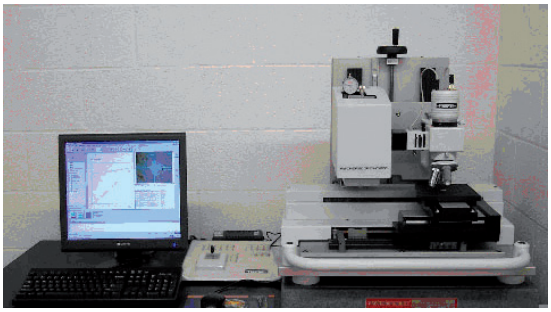

Figure 3. The Fischerscope HM2000 indenter (Mechanical Engineering Department, Texas A&M University).

A different way to determine the hardness is by means of plotting the values of the test load against the indentation depth. Besides the hardness value, this plot is able to deliver characteristics such as the modulus of elasticity, plastic hardness, and the plastic and elastic parts of the indentation work.

Despite the mature state of evolution of nanoindentation test instruments, the process of undertaking such a test requires considerable experimental skill and resources. The tests are extremely sensitive to thermal expansion and contraction due to temperature changes and mechanical vibration during testing. It is necessary to ensure that the specimen and the instrument are in thermal equilibrium. For example, handling the specimen or the indenter requires a reasonable delay before beginning the indentation so that errors are not introduced into the displacement measurements by virtue of thermal expansion or contraction during the test resulting from the contact with external sources or sinks of heat.

Specimens are typically mounted on a metal base with wax or mounting adhesive. The specimen holder is in turn placed on a stage. Stage movement is usually controlled by motorized axes that have a resolution, or step size, of less than 0.5 μm. Such fine positioning is usually needed to allow indentations to be made on very small features, such as grains in a ceramic or conductive pads in an integrated circuit. Stage movement is usually servo-controlled with proportional, integral, and derivative gains that can be set to allow for the most precise positioning.

Nanoindentation hardness tests are generally made with either spherical or pyramidal indenters. Consider a Vickers indenter with opposing faces at a semi-angle of $\theta = 68°$ and therefore making an angle $\beta = 22°$ with the flat specimen surface. For a particular contact radius a, the radius R of a spherical indenter whose edges are at a tangent to the point of contact with the specimen is given by $\sin\beta = a/R$, which for $\beta = 22°$ gives $a/R = 0.375$.

For a Vickers diamond pyramid indenter (a square pyramid with opposite faces at an angle of 136° and edges at 148° and face angle of 68°), the Vickers diamond hardness (VDH) is calculated using the indenter load and the actual surface area of the impression. The VDH is lower than the mean contact pressure by around 7%; the hardness is found from:

$$\mathrm{VDH} = \frac{2P}{d^2}\sin\frac{136°}{2} \tag{2}$$

with d equal to the length of the diagonal measured from corner to corner of the residual impression on the specimen surface. Traditionally, Vickers hardness is calculated using eqn 2 with d in mm and P in kgf .

To recapitulate, the principal goal of nanoindentation testing is to extract the elastic modulus and hardness of the specimen material from experimental readings of indenter load and depth of penetration. In a typical test, force and depth of penetration are recorded as load is applied from zero to some maximum and then back to zero. If plastic deformation occurs, a residual impression is left on the surface of the specimen. Unlike with conventional indentation hardness tests, the size (and hence the projected contact area) of the residual impression made by nanoindentation testing is too small to measure accurately using optical techniques. The depth of penetration together with the known geometry of the indenter provides an indirect measure of the area of contact at full load, from which the mean contact pressure, and thus the hardness, may be estimated. When the load is removed from the indenter, the material attempts to regain its original shape, but it prevented from doing so because of plastic deformation. However, there is some degree of recovery due to the relaxation of elastic strains within the material. An analysis of the initial portion of this elastic unloading response gives an estimate of the elastic modulus of the indented material.

5. Simulation of the structural integrity of the diamond wheel

3D modelling of the structural integrity of the diamond wheel was carried out in two stages—the calculation of the entire construction and calculations of the integrity of the diamond layer (Figure 4).

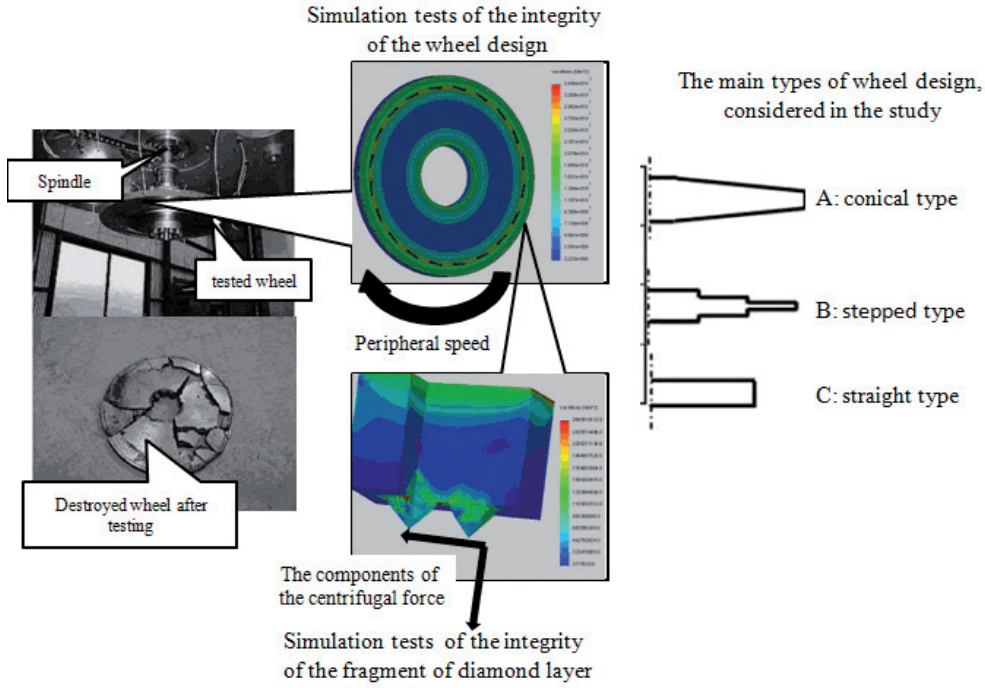

Figure 4. Overall concept of 3D modelling of the structural integrity of high-speed grinding wheels.

Tensile testing of specimens of diamond layers containing various combinations of diamond grains and binders was undertaken to validate the models.

Improving the reliability of construction components and machine parts makes high demands on design decisions, because the structure must on the one hand be strong enough and, if necessary, rigid and stable and on the other hand have the lowest possible consumption of materials, complexity and manufacturing cost.

To a large extent this problem can be solved by rational design based on modern methods of strength calculations. It must be ensured that the highest stress in the cross-section of the designed element that emerges at a given load is below the limit of the stress at which there is a risk of plastic deformation or fracture.

For the plastic materials of the wheel base, the tensile and compressive stress limit is the yield strength. Hence, for them the allowable stress $[\sigma]$ is obtained from the yield strength σ_T of the material:

$$[\sigma] = \frac{\sigma_T}{n}, \tag{3}$$

where n is a safety factor. For brittle materials, the allowable tensile stress σ_t and the allowable compressive stress σ_c are obtained based on the corresponding ultimate (subscript u) strengths σ_{tu} and σ_{cu}:

$$[\sigma_t] = \frac{\sigma_{tu}}{n} \text{ and } [\sigma_c] = \frac{\sigma_{cu}}{n}. \tag{4}$$

Safety factors with respect to temporary withstanding of brittle strength during dynamic operation should be chosen to be quite large. This is due to the fact that exceeding the maximum ultimate stress even just once causes destruction. The safety factor can be calculated using the finite element method in the software package Abaqus using the maximum normal stresses σ_{norm}, and should of course be less than unity:

$$\frac{\sigma_{norm}}{\sigma_u} < 1. \tag{5}$$

6. Results

Simulation results for some nanoindentation tests are shown in Figure 5.

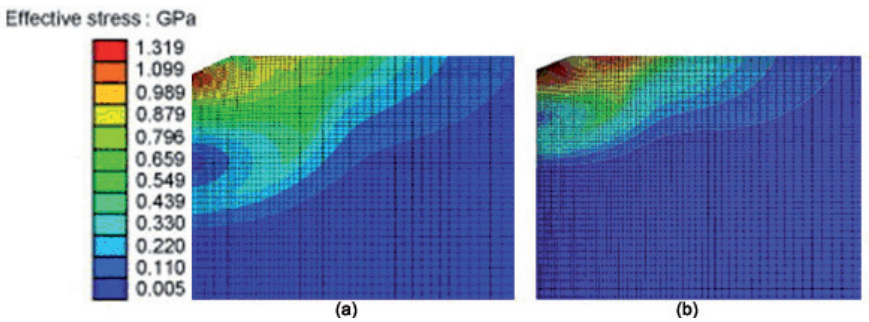

Figure 5. Nanoindentation simulation results for: (a) Bakelite binder with a measured elastic modulus of 550.8 N/mm^2; (b) for iron-based binder with a measured elastic modulus of 200.470 N/mm^2.

The form of the compliance curves for different binders are very similar. Figure 6 shows the experimental results of nanohardness measurements for the Bakelite and iron-based binders.

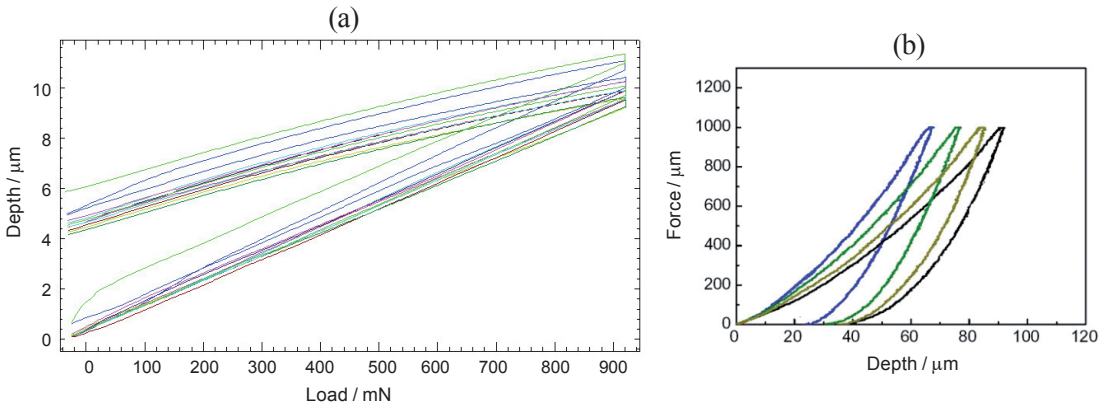

Figure 6. Nanohardness measurements for: (a) Bakelite binder with a measured elastic modulus of 530.6 N/mm^2; (b) iron-based binder with a measured elastic modulus of 200.0 kN/mm^2. Different colours indicate different experiments on a given sample.

Figure 7 shows the microstructure of the diamond grinding wheel.

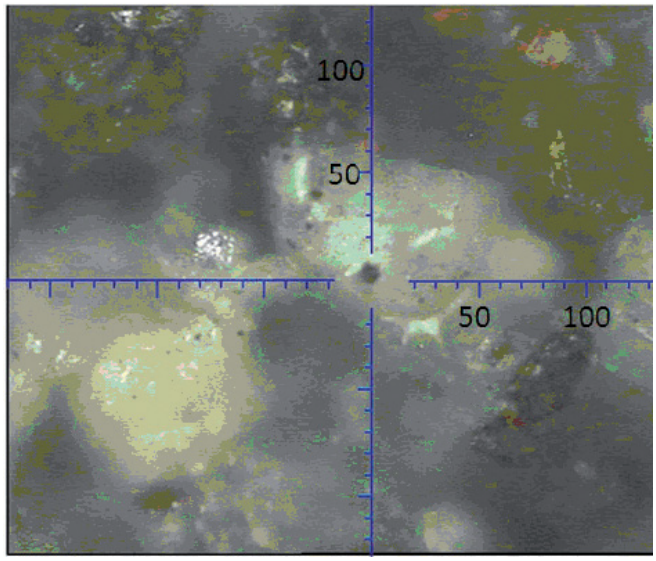

Figure 7. Microstructure of the diamond layer showing grains, metal inclusions and porosity. Images were obtained using the Fischerscope HM2000 (Figure 3). The numbers give distances in μm.

Mechanical properties of various binders were determined using nanoindentation measurements and the images of the microstructure of the diamond layer were used to refine the model simulating the structural integrity of the diamond wheel.

Using our experimental data on nanoindentation and from the tensile tests of diamond layer samples, a series of model integrity-determining experiments on the influence of the shape and physical and mechanical properties of the diamond wheel were carried out, the results of which are shown in Figure 8.

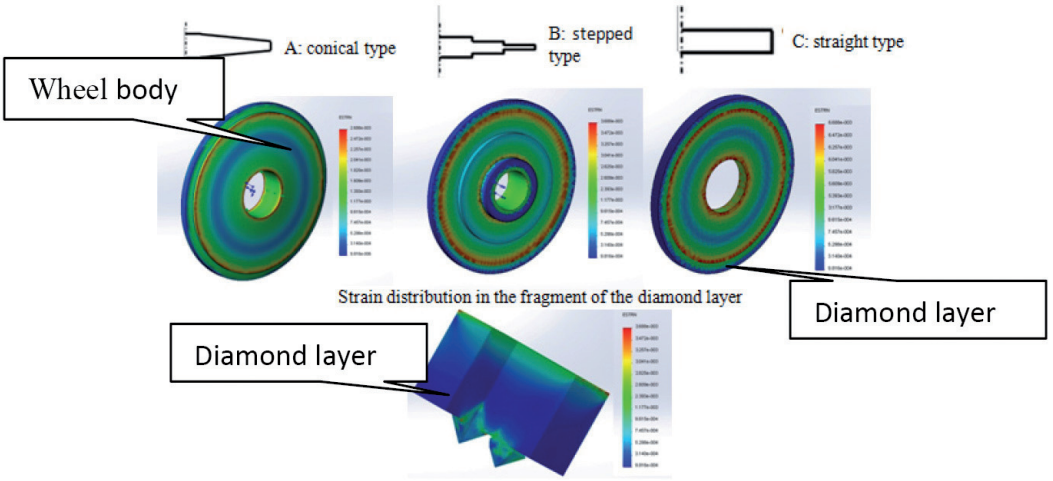

Figure 8. Distribution of deformations in the components of the wheel during the action of significant centrifugal forces during high speed grinding. The material of the wheel body was light aluminium alloy and the diamond layer had an iron-based binder. The peripheral speed for all three wheel types was 150 m/s. The greatest strain values (red) are observed in the cases C, 0.75 μm; B, 0.51 μm; A, 0.45 μm. The wheel, in this case, includes the body and the diamond layer glued together.

The results of these calculations have been confirmed by studies,[8] carried out with the help of a high-speed spindle, which allowed a peripheral speed of 500 m/s to be attained for wheels with a diameter of 200 mm. Figure 9 shows the correlation of the results of FEM calculations and experiments using rotational speeds ranging from 50 to 200 m/s.

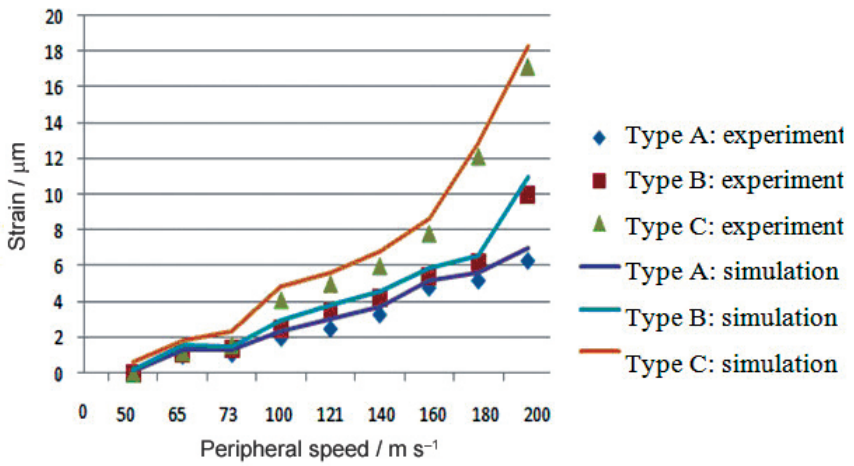

Figure 9. Dependence of strains in the wheel *vs* peripheral speed (see text).

7. Discussion

Experimental results for the nanoindentation test showed good convergence of the simulation with the experiments (Figures 5 and 6). It is, therefore, considered to be appropriate and useful to use nanoindentation modelling to study the structure of grinding wheels for further research into practical applications. The developed and tested model will be used to investigate the coating of diamond grains. Since the diamond grain has a complicated form it is not possible to prepare a corresponding sample for the experimental setup.

The results calculated from modelling the structural integrity of the wheel indicate the feasibility of using a stepped or cone structure in order to reduce the internal stresses and strains; this will increase the stability of processing at high speeds (Figures 8 and 9). Using these forms of diamond grinding wheels, strain is reduced and the initial shape of the tool is retained at high processing speeds. This improves the stability of the high-speed diamond grinding process, reduces the cost of development and obviates the necessity for the installation of additional rigidity systems for supporting equipment.

The use of high-speed tools requires stability and safety at work. To confirm the safety of the diamond wheel at different processing speeds, simulations were conducted and diagrams of safety factor distribution depending on the shape and structure of the tool were obtained (Figure 10). From these calculations it can be inferred that the integrity of the rotating wheel at a peripheral speed up to 420 m/s is assured. The optimal design types in this case are conical or stepped, which have the greatest values of the safety factor (respectively 3.45 and 3.11) for peripheral speeds up to 300 m/s.

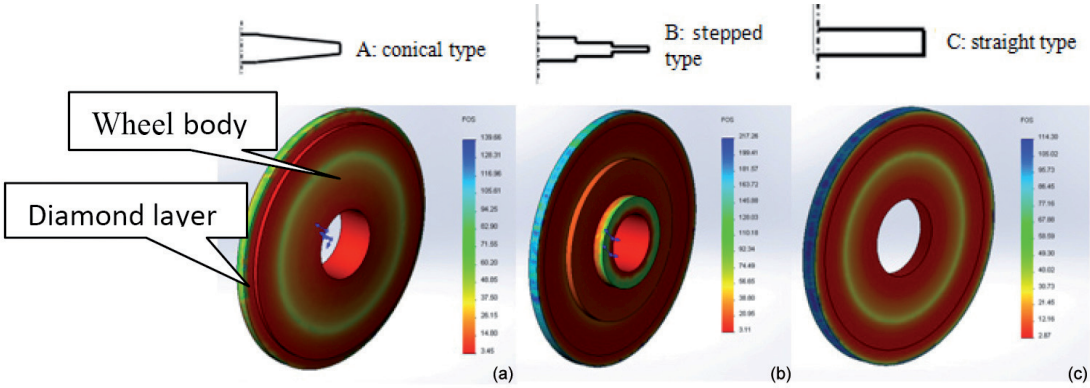

Figure 10. Distribution of safety factor (equation 5) depending on the design of the wheel for a peripheral speed of 300 m/s. The wheel body material was lightweight aluminum-based alloy and the binder of the diamond layer was an iron-based alloy. (a) minimum safety factor = 3.45; (b) minimum safety factor = 3.11; (c) minimum safety factor = 2.61. Red indicates the places having the largest value of the safety factor.

8. Summary and conclusions

Summarizing the main experimental and simulation results pertaining to the optimization of the structure of the diamond wheel used in high speed grinding, the following concluding remarks may be drawn:

1 A 3D methodology for determining the strength characteristics of diamond wheels for high-speed grinding was developed, the performance of which was confirmed by experiment.
2 By calculation, diagrams of the safety factor distribution for a range of materials, test modes and wheel designs were obtained.
3 The calculation results indicate the feasibility of using a stepped or cone structure for the wheel in order to reduce internal stresses and strains, thereby increasing the stability of high-speed processing.
4 Images of the microstructure of the diamond layer with different binders were used to refine the numerical model.

Acknowledgment

D.V. Romashov and D.O. Fedorenko wish to express their gratitude for financial and technical support of this research to the Ministry of Education and Science of the Ukraine.